# $CO_2$ Semi-annual Oscillation in the Middle Troposphere and at the Surface

Xun Jiang[1*], Moustafa T. Chahine[2], Qinbin Li[3], Maochang Liang[4], Edward T. Olsen[2], Luke L. Chen[2], Jingqian Wang[1], and Yuk L. Yung[5]

[1] Department of Earth & Atmospheric Sciences, University of Houston, USA

[2] Science Division, Jet Propulsion Laboratory, California Institute of Technology, USA

[3] Department of Atmospheric and Oceanic Sciences, UCLA, USA.

[4] Research Center for Environmental Changes, Academia Sinica, Taipei, Taiwan.

[5] Division of Geological and Planetary Sciences, California Institute of Technology, Pasadena, USA.

[*] To whom all correspondence should be addressed. E-mail: xjiang4@mail.uh.edu

**Submitted to GBC Aug 9, 2010; Revise May 21, 2011**

**Abstract:**

Using in-situ measurements, we find a semi-annual oscillation (SAO) in the mid-tropospheric and surface $CO_2$. Chemistry-transport models (2-D Caltech/JPL model, 3-D GEOS-Chem, and 3-D MOZART-2) are used to investigate possible sources for the SAO signal in the mid-tropospheric and surface $CO_2$. From model sensitivity studies, it is revealed that the SAO signal in the mid-tropospheric $CO_2$ mainly originates from surface $CO_2$ with a small contribution from transport fields. It is also found that the source for the SAO signal in surface $CO_2$ is mostly related to the $CO_2$ exchange between biosphere and atmosphere. By comparing model $CO_2$ with in-situ $CO_2$ measurements at surface, we find that models are able to capture both annual and semi-annual cycles well at surface. Models can also simulate annual and semi-annual cycles of mid-tropospheric $CO_2$ reasonably well in the tropical region by comparison with aircraft measurements.

## 1. Introduction

Atmospheric $CO_2$ has a global trend of ~2 ppm/year [*Keeling et al*., 1995]. The increasing of atmospheric $CO_2$ has a significant impact on the global climate change [*Dickinson and Cicerone*, 1986]. Superimposed upon this trend is an annual cycle resulting from the uptake and release of $CO_2$ by vegetation whose amplitude is greatest in the northern hemisphere (NH). Using $CO_2$ measurements at Mauna Loa, Buermann *et al*. [2007] found that variations of $CO_2$ seasonal cycle amplitudes are closely related to the carbon sequestration in the biosphere, and are influenced by precipitation and circulation. In addition to the trend and annual cycle, atmospheric $CO_2$ also shows intra-seasonal and inter-annual variabilities.

El Niño is the most important tropical interannual variability that can influence the $CO_2$ concentrations. During El Niño (La Niña) events, the atmospheric $CO_2$ growth rate increases (decreases) at tropical surface stations [*Keeling et al*., 1995; *Jones et al.*, 2001; *Nevison et al*., 2008]. Using mid-tropospheric $CO_2$ data from AIRS, Jiang *et al*. [2010] found that El Niño can influence the mid-tropospheric $CO_2$. Mid-tropospheric $CO_2$ is enhanced in central Pacific Ocean and diminished in the western Pacific Ocean during El Niño [*Jiang et al*., 2010]. In the high latitudes, mid-tropospheric $CO_2$ concentration can be influenced by the strength of the polar vortex. Polar mid-tropospheric $CO_2$ is reduced (enhanced) when the polar vortex is strong (weak) [*Jiang et al*., 2010]. Recently, Li *et al*. [2010] demonstrate that mid-tropospheric $CO_2$ concentrations can be influenced by the Madden-Julian Oscillation.

In this paper, we will focus on investigating the intra-seasonal variability of mid-tropospheric $CO_2$, especially on the semi-annual oscillation (SAO) of $CO_2$ and its possible sources. This work will yield a quantitative study of how SAO influences the mid-tropospheric $CO_2$. It also offers an opportunity to investigate the possible source for the SAO signal in the mid-tropospheric $CO_2$.

## 2. Data and Models

In this paper, we use aircraft $CO_2$ from *Matsueda et al*. [2002], which are incorporated into Comprehensive Observation Network for Trace gases by AIrLiner (CONTRAIL). Aircraft $CO_2$ from *Matsueda et al*. [2002] are measured at 8-13 km biweekly since April 1993 to present. $CO_2$ over the western Pacific from Australia to Japan are measured. The latitudinal coverage is approximately from 25°S to 35°N. The longitudinal coverage is from 135°E to 150°E. We also use surface $CO_2$ flask measurements from NOAA ESRL network [*Tans et al*. 1998; *GLOBALVIEW-$CO_2$*, 2007]. Site information for NOAA surface $CO_2$ is available at http://www.esrl.noaa.gov/gmd/dv/site/site_table.html.

To investigate possible sources of the semi-annual oscillation of mid-troposphere and surface $CO_2$, we use three different chemistry-transport models. These models are the Caltech/JPL 2-D chemistry-transport model (CTM) [*Shia et al*., 2006], 3-D GEOS-Chem [*Suntharalingam et al*., 2004], and 3-D MOZART-2 [*Horowitz et al*., 2003]. The 2-D CTM has 18 latitudes, equally spaced from pole to pole. It has 40 vertical layers, equally spaced in log scale of pressure from the surface to the upper boundary at 0.01 hPa. Transport in the model is by the stream function and the horizontal and vertical diffusivities taken from *Jiang et al*. [2004]. The stream function is derived from the National Center for Climate Prediction (NCEP) Reanalysis 2 data [*Jiang et al*., 2004]. An important feature of the 2-D CTM is its ability to reproduce the age of air in the stratosphere [*Morgan et al*., 2004].

GEOS–Chem (v7.3.3) is driven by the Goddard Earth Observing System (GEOS-4) assimilated meteorological data from the NASA Global Modeling Assimilation Office (GMAO). Spatial resolution for GEOS-Chem is 2° (latitude) × 2.5° (longitude). There are 30 levels in the vertical from the surface to about 0.01 hPa (~70 km). Advection is computed every 15 minutes with a flux-form semi-Lagrangian method [*Lin and Rood*, 1996]. Moist convection is computed using the GEOS convective, entrainment, and detrainment mass fluxes described by *Allen et al.* [1996a, 1996b]. The physics in the GEOS-4 analysis system is adopted from the National Center for Atmospheric Research (NCAR) Community Climate Model, Version 3 (CCM3) and Whole Atmosphere

Community Climate Model (WACCM) with important modifications to make it suitable for data assimilation [*Bloom et al*., 2005].

MOZART-2 is driven by the meteorological inputs every 6 hours from the NCEP Reanalysis 1 [*Kalnay et al.*, 1996]. Advection is computed every 20 minutes with a flux-form semi-Lagrangian method [*Lin and Rood*, 1996]. The horizontal resolution is 2.8° (latitude) × 2.8° (longitude) with 28 vertical levels extending up to approximately 40 km altitude [*Horowitz et al*., 2003]. MOZART-2 is built on the framework of the Model of Atmospheric Transport and Chemistry (MATCH). MATCH includes representations of advection, convective transport, boundary layer mixing, and wet and dry deposition.

Surface emissions and vertical transport in CTMs are both crucial for $CO_2$ simulation in the free troposphere. We will use two different boundary conditions to investigate how boundary conditions affect the mid-tropospheric $CO_2$. The GLOBALVIEW-$CO_2$ mixing ratio data [*Tans et al*. 1998; *GLOBALVIEW-$CO_2$*, 2007] is used as the lower boundary condition for the Caltech/JPL CTM, GEOS-Chem, and MOZART-2. For convenience, we refer this hereforth as the GLOBALVIEW-$CO_2$ boundary condition [*Jiang et al*., 2008]. Since the GLOBALVIEW-$CO_2$ data are limited in space, especially over ocean, we used the GLOBALVIEW-$CO_2$ to rescale the $CO_2$ mixing ratio at the surface for the GLOBALVIEW-$CO_2$ boundary condition. First, monthly mean model $CO_2$ mixing ratios at surface are regressed against GLOBALVIEW-$CO_2$ surface flask measurements. Then model surface $CO_2$ mixing ratios are rescaled by the scale derived from regression. The monthly mean GLOBALVIEW-$CO_2$ flask data are close to the GLOBALVIEW-$CO_2$ boundary condition when they are co-located.

We will also use the prescribed $CO_2$ sources and sinks as the boundary condition for GEOS-Chem and MOZART-2. The exchange of $CO_2$ between the terrestrial biosphere and atmosphere is based on net primary productivity and respiration fluxes from the Carnegie-Ames-Stanford (CASA) ecosystem model [*Randerson et al*., 1997]. Monthly mean biospheric $CO_2$ fluxes from 2000 to 2004 are used in the models. Air-to-sea exchange of $CO_2$ is from *Takahashi et al*. [1997]. Estimates of fossil fuel emissions are

from *Marland et al.* [2007]. Monthly mean biomass burning emissions of $CO_2$ are derived based on *Duncan et al*. [2003]. Since there is an unbalanced $CO_2$ budget associated with the prescribed source and sink boundary condition [*Suntharalingam et al.*, 2003; *Suntharalingam et al.*, 2004], we regress surface $CO_2$ mixing ratio in the GEOS-Chem restart file against the GLOBALVIEW-$CO_2$ surface flask measurements. As a result, the unbalanced $CO_2$ budget is resolved to some degree [*Jiang et al*., 2008]. Discrepancies between the model $CO_2$ simulations (driven by the same meteorological fields) with the above-mentioned two boundary conditions would help identify potential issues with the surface sources and/or sinks on simulating $CO_2$ annual and semi-annual cycles.

## 3. Results

Figure 1 presents a comparison between Matsueda's aircraft $CO_2$ (red dots) and model $CO_2$ mixing ratios averaged between 9 km and 13 km (solid lines) from 2000 to 2004. The panels are for 25°S, 15°S, 5°S, 5°N, 15°N, and 25°N, respectively. Different color lines are for different model simulations. There are two GEOS-Chem model outputs. One is forced by the GLOBALVIEW-$CO_2$ boundary condition (green line). The other is forced by the prescribed $CO_2$ sources and sinks boundary condition (orange line). GEOS-Chem $CO_2$ forced by the prescribed $CO_2$ source/sink boundary condition (orange line) have higher $CO_2$ concentrations in the summer seasons than that forced by GLOBALVIEW-$CO_2$ boundary condition (green line). It suggests that there might be a missing sink in the prescribed $CO_2$ source/sink boundary condition in the summer season. Purple line is $CO_2$ from Caltech 2D model. Blue line is $CO_2$ from MOZART2 forced by NCEP1 meteorology. The model results match the high precision aircraft measurements of $CO_2$ in the middle troposphere remarkably well. Seasonal cycle and trend for $CO_2$ are simulated well by different models. The amplitude of $CO_2$ seasonal cycle increases with latitudes, with larger seasonal cycle in the northern hemisphere compared with that in the southern hemisphere. In addition to the annual cycle, there is a six-month signal appearing in the $CO_2$ from both aircraft and model simulations. To investigate the six-month signal in more details, power spectral analysis is applied to the detrended $CO_2$

from aircraft and model simulations. Linear trends have been removed from $CO_2$ time series. Power spectra for the detrended $CO_2$ are shown in Figure 2. In addition to the spectral peak at 12 months, 6-month signal appears in both Matsueda's $CO_2$ and model $CO_2$.

To investigate sources of the semi-annual oscillations in the mid-tropospheric $CO_2$, we first apply sensitivity studies to the 2-D Caltech/JPL chemistry and transport model. Averaged $CO_2$ at 9-13 km forced by the GLOBALVIEW-$CO_2$ boundary condition and NCEP2 Meteorology field is shown by solid line in Figure 3. To investigate the annual cycle and semi-annual cycle amplitudes in the mid-tropospheric $CO_2$, we fit the data by a series of Legendre polynomials and harmonic functions [*Jiang et al.,* 2008]. We use the sum of the first, second, and third Legendre polynomials to remove the trend from the data. The harmonic functions represent annual and semi-annual cycles. Annual cycle, calculated by $e\cos(2\pi t) + f\sin(2\pi t)$, is shown in Fig. 3b, where $e$ and $f$ are the amplitudes of the annual cycle. The amplitude for the annual cycle of 2-D model $CO_2$ at 25°N is about 2.3 ppm. Semi-annual cycle, calculated by $g\cos(4\pi t) + h\sin(4\pi t)$, is shown in Fig. 3c, where $g$ and $h$ are the amplitudes of the semi-annual cycle. The amplitude for the semi-annual cycle of 2-D model $CO_2$ at 25°N is about 0.8 ppm. In a sensitivity test, we removed the annual and semi-annual oscillations from surface $CO_2$ and used linear trends as the boundary condition at the model surface. As such, there is no semi-annual cycle and annual cycle source originating from surface in this model run. This results in the reduction of the amplitude of semi-annual cycle for mid-tropospheric $CO_2$ to 0.09 ppm, which is about 11% of the total amplitude of the semi-annual oscillation in the mid-tropospheric $CO_2$. It clearly suggests that the dominant source for the semi-annual cycle in the middle troposphere is propagated from the surface sources. Weak semi-annual and annual cycles in the mid-tropospheric $CO_2$ shown by dashed lines in Figs. 3b and 3c originate from transport fields. The phase of the $CO_2$ seasonal cycle due to the transport (dashed line in Figure 3b) is shifted relative to that forced by the GLOBALVIEW-$CO_2$ boundary condition and NCEP2 reanalysis meteorology field (solid line in Figure 3b). The $CO_2$ seasonal signal due to the transport (dashed line in Figure 3b) is related to the strength of the vertical velocity in the 2D CTM. The vertical velocity is

stronger in the summer season and weaker in the winter season. More $CO_2$ can be lifted to the middle-troposphere during the summer than in the winter season. Thus mid-tropospheric $CO_2$ (dashed line in Figure 3b) reaches maximum value in the summer season at 25°N. Phase for the $CO_2$ seasonal cycle (forced by the GLOBALVIEW-$CO_2$ boundary condition and NCEP2 reanalysis meteorology field; solid line in Figure 3b) represents the contribution from surface $CO_2$ sources, which reach maximum in April. In another sensitivity test, we force the model with linear $CO_2$ trend boundary condition and climatological transport fields. Climatological transport fields are the average of the transport fields from 2000 to 2004. There is no semi-annual oscillation originating from either the surface or the transport fields. As a result, semi-annual oscillation disappears in mid-tropospheric $CO_2$ as shown by the dotted line in Fig. 3c. In independent sensitivity studies, we also find that the semi-annual oscillation in the mid-tropospheric $CO_2$ originates from the surface semi-annual cycles and not the surface annual cycles.

Annual and semi-annual oscillations in surface $CO_2$ are also examined. Similar spectral analysis is applied to the GLOBALVIEW-$CO_2$ and GEOS-Chem model $CO_2$ at the surface. In addition to the annual cycle, semi-annual oscillation signals are also present in the surface $CO_2$ from GLOBALVIEW-$CO_2$ and model $CO_2$. To compare the annual cycle and semi-annual cycle amplitudes in surface $CO_2$ from observations and model results, we calculate the annual cycle amplitude ($\sqrt{e^2+f^2}$) and semi-annual cycle amplitude ($\sqrt{g^2+h^2}$) for surface $CO_2$ from GLOBALVIEW network and GEOS-Chem model output. Results are shown in Figure 4. The amplitudes for annual and semi-annual cycles from GEOS-Chem $CO_2$ are very close to those from GLOBALVIEW-$CO_2$ at the surface. The amplitudes of annual and semi-annual cycles are larger in the northern hemisphere compared with those in the southern hemisphere. The maximum amplitude for the annual cycle of surface $CO_2$ is about ~10 ppm. The maximum amplitude is about ~3.5 ppm for the semi-annual cycle of surface $CO_2$. Scatter plots of the observed and model simulated amplitudes for semi-annual cycle and annual cycle of surface $CO_2$ are shown in Figure 5. As revealed in Figure 5, the GEOS-Chem model seems to over-estimate the semi-annual oscillation amplitudes compared with those from observations. The latitudinal

distributions of the amplitudes for the semi-annual and annual cycles are shown in Figure 6. The amplitude increases with latitude, which appears from both surface GLOBALVIEW-$CO_2$ data and models. Semi-annual and annual cycle amplitudes are larger in the northern hemisphere than those in the southern hemisphere. This is because semi-annual and annual cycles in surface $CO_2$ sources (e.g. the net exchange between biosphere and atmosphere) are larger in the northern hemisphere than those in the southern hemisphere.

To investigate possible sources for the semi-annual oscillation of $CO_2$ at the surface, we examine the signals from different $CO_2$ surface sources, which include biomass burning, fossil fuel emission, ocean, and biosphere. Fossil fuel emission contributes to the positive trend in $CO_2$. $CO_2$ semi-annual cycle and annual cycle are mainly from exchange between the atmosphere and the biosphere. Biomass burning also contributes to the semi-annual cycle of $CO_2$. Gross primary production, respiration, and net ecosystem production at 30°N and 110°E, shown in Figure 7, are an example to illustrate the semi-annual oscillation in $CO_2$ source from the biosphere. Gross primary production (Fig. 7a), is related to carbon uptake by plants during photosynthesis. The values are negative since $CO_2$ is uptaken by vegetation from the atmosphere. Ecosystem respiration (Fig. 7b), is related to the autotrophic and heterotrophic respirations from biosphere. In the winter season, photosynthesis is largely reduced. The peak for gross primary production (Fig. 7a), is relatively flat in winter. However, there are still $CO_2$ emitted to the atmosphere by respirations from the biosphere in winter, which has a relatively sharp peak compared with the photosynthesis term. The sum of the two terms, gross primary production and ecosystem respiration, leads to the double peaks in each year in the net ecosystem production, as shown in Fig. 7c. Thus, phase differences in the gross primary production (photosynthesis) and ecosystem respiration lead to the semi-annual oscillation in $CO_2$ at surface. Surface semi-annual oscillation can propagate to the middle-troposphere, which is the dominant source for the semi-annual oscillation in the mid-tropospheric $CO_2$.

## 4. Conclusions

In addition to the annual cycle, the semi-annual oscillation of mid-tropospheric and surface $CO_2$ is discussed in this paper by combining the in-situ measurements with chemistry-transport models. Chemistry and transport models, driven by different transport schemes, are used to simulate the middle tropospheric $CO_2$. We also apply different boundary conditions to force the 3-D CTMs. The seasonal cycle and semi-annual oscillation of surface $CO_2$ are well simulated by chemistry-transport model with the prescribed $CO_2$ sources and sinks boundary condition. Semi-annual oscillation is also found in the mid-tropospheric $CO_2$. From the sensitivity study, we found that the semi-annual oscillation in the mid-tropospheric $CO_2$ is mainly originated from sources at surface. Possible reason for the semi-annual oscillation of surface $CO_2$ is the $CO_2$ surface source due to net ecosystem production.

Acknowledgement: We thank two anonymous reviewers and the associate editor for the helpful comments. Dr. Jiang is supported by JPL Grant G99694. Dr. Liang is supported by an NSC grant 98-2111-M-001-014-MY3 to Academia Sinica. Dr. Yung is supported by JPL Grant P765982 to the California Institute of Technology.

**References:**


Allen, D. J., R. B. Rood, A. M. Thompson, and R. D. Hidson (1996a), Three-dimensional $^{222}Rn$ calculations using assimilated data and a convective mixing algorithm, *J. Geophys. Res.*, *101*, 6871-6881.

Allen, D. J., *et al*. (1996b), Transport induced interannual variability of carbon monoxide using a chemistry and transport model, *J. Geophys. Res.*, *101*, 28655-28670.

Bloom, S., *et al*. (2005), The Goddard Earth Observation System Data Assimilation System, GEOS DAS Version 4.0.3: Documentation and Validation, NASA TM-2005-104606, *26*, 166pp.

Dickinson, R. E., and R. J. Cicerone (1986), Future global warming from atmospheric trace gases, *Nature, 319*(6049), 109-115.

Buermann, W., *et al.* (2007), The changing carbon cycle at Mauna Loa Observatory, *Proceedings of the National Academy of Sciences of the United States of America*, doi:10.1073/pnas.0611224104.

Duncan, B. N., *et al*. (2003), Interannual and seasonal variability of biomass burning emissions constrained by satellite observations, *J. Geophys. Res.*, *108*, doi:10.1029/2002JD002378.

GLOBALVIEW-$CO_2$ (2007), *Cooperative Atmospheric Data Integration Project: Carbon Dioxide* [CD-ROM], NOAA ESRL, Boulder, Colorado (Also available on Internet via anonymous FTP to ftp.cmdl.noaa.gov, Path: ccg/co2/GLOBALVIEW)

Horowitz, L. W., *et al*. (2003), A global simulation of tropospheric ozone and related tracers: description and evaluation of MOZART, version 2, *J. Geophys. Res.*, *108*, doi:10.1029/2002JD002853.

Jiang, X. C. D. Camp, R. Shia, D. Noone, C. Walker, and Y. L. Yung (2004), Quasi-biennial oscillation and quasi-biennial oscillation-annual beat in the tropical total column ozone: A two-dimensional model simulation, *J. Geophys. Res.*, *109*, Art. No. JD004377.

Jiang, X., Q. Li, M. Liang, R. Shia, M. T. Chahine, E. T. Olsen, L. Chen, and Y. L. Yung (2008), Simulation of upper tropospheric CO2 from chemistry and transport models, *Global Biogeochemical Cycles*, *22*, doi:10.1029/2007GB003049.

Jiang, X., M. T. Chahine, E. T. Olsen, L. L. Chen, and Y. L. Yung (2010), Interannual variability of mid-tropospheric $CO_2$ from Atmospheric Infrared Sounder, *Geophysical Research Letters, 37*, doi:10.1029/2010GL042823.

Jones, C. D., M. Collins, P. M. Cox, and S. A. Spall (2001), The carbon cycle response to ENSO: A coupled climate-carbon cycle model study, *Journal of Climate*, *14*, 4113-4129.

Kalnay, E., *et al.* (1996), The NCEP/NCAR 40-year reanalysis project, *Bull. Am. Meteorol. Soc*., *77*, 437-471.

Keeling, C. D., T. P. Whorf, M. Wahlen, and J. Vanderplicht (1995), Interannual extremes in the rate of rise of atmospheric carbon dioxide since 1980, *Nature*, *375*, 666-670.

Li, K. F., B. Tian, D. E. Waliser, and Y. L. Yung (2010), Tropical mid-tropospheric CO2 variability driven by the Madden-Julian Oscillation, *Submitted to PNAS.*

Lin, S. J., and R. B. Rood (1996), Multidimensional flux form semi-Lagrangian transport schemes, *Mon. Weather Rev.*, *124*, 2046-2070.

Marland, G., T. A. Boden, and R. J. Andres, Global, Regional, and National $CO_2$ Emissions. In *Trends: A Compendium of Data on Global Change*. *Carbon Dioxide Information Analysis Center*, Oak Ridge National Laboratory, U.S. Department of Energy, (Oak Ridge, TN, 2007).

Matsueda, H., H. Y. Inoue, and M. Ishii (2002), Aircraft observation of carbon dioxide at 8-13 km altitude over the western Pacific from 1993 to 1999, *Tellus*, *54B*(1), 1-21. The data are available at http://gaw.kishou.go.jp/wdcgg.html

Morgan, C. G., *et al*. (2004), Isotopic fractionation of nitrous oxide in the stratosphere: Comparison between model and observations, *J. Geophys. Res.*, *109*, D04305.

Nevison, C. D., *et al*. (2008), Contribution of ocean, fossil fuel, land biosphere, and biomass burning carbon fluxes to seasonal and interannual variability in atmospheric CO2, *Journal of Geophysical Research*, 113, doi:10.1029/2007JG000408.

Randerson, J. T., *et al*. (1997), The contribution of terrestrial sources and sinks to trends in the seasonal cycle of atmospheric carbon dioxide, *Global Biogeochem. Cycles*, *11*, 535-560.

Shia, R., M. Liang, C. E. Miller, and Y. L. Yung (2006), $CO_2$ in the upper troposphere: influence of stratosphere-troposphere exchange, *Geophys. Res. Lett., 33*, doi:10.1029/2006GL026141.

Suntharalingam, P., *et al*. (2003), Estimating the distribution of terrestrial CO2 sources and sinks from atmospheric measurements: sensitivity to configuration of the observation network, *J. Geophys. Res.*, *108*, doi:10.1029/2002JD002207.

Suntharalingam, P., *et al*. (2004), Improved quantification of Chinese carbon fluxes using CO2/CO correlations in Asian outflow, *J. Geophys. Res.*, *109*(D18), doi:10.1029/2003JD004362.

Takahashi, T., *et al*. (1997), Global air-sea flux of CO2: An estimate based on measurements of sea-air pCO2 difference, *Proc. Natl. Acad. Sci. U. S. A.*, *94*, 8929.

Tans, P.P., *et al*. (Eds.) (1998), Carbon Cycle, in *Climate Monitoring and Diagnostics Laboratory No. 24 Summary Report 1996-1997*, edited by D.J. Hoffmann *et al*., chap. 2, pp. 30-51, NOAA Environ. Res. Lab., Boulder Colo. (Data available from http://www.cmdl.noaa.gov/)

Figure 1: Aircraft observations between 9 km and 13 km (red dots) [Matsueda *et al.*, 2002] and model $CO_2$ mixing ratios (color lines). The $CO_2$ mixing ratios from the GEOS-chem model forced by GLOBALVIEW-$CO_2$ boundary condition (BC) and prescribed $CO_2$ source/sink BC are shown by the green and orange lines, respectively. The $CO_2$ mixing ratio from the Caltech/JPL 2-D model forced by NCEP2 and GLOBALVIEW-$CO_2$ BC are shown by purple line. The $CO_2$ mixing ratios from MOZART-2 forced by NCEP1 and GLOBALVIEW-$CO_2$ BC are shown by the blue line.

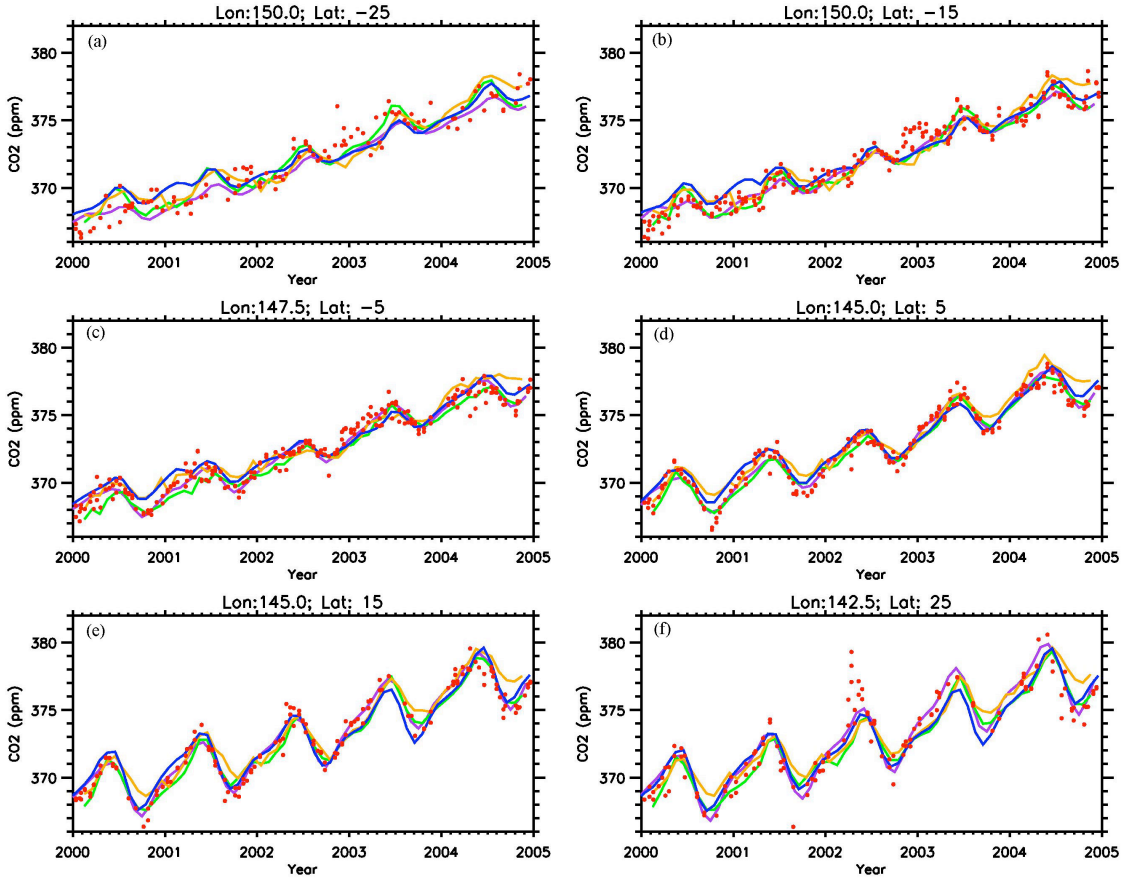

Figure 2: Power spectra for aircraft and model $CO_2$ time series. Red dash line is the power spectra for the Matsueda's data. Colors for solid lines are the same as in Figure 1.

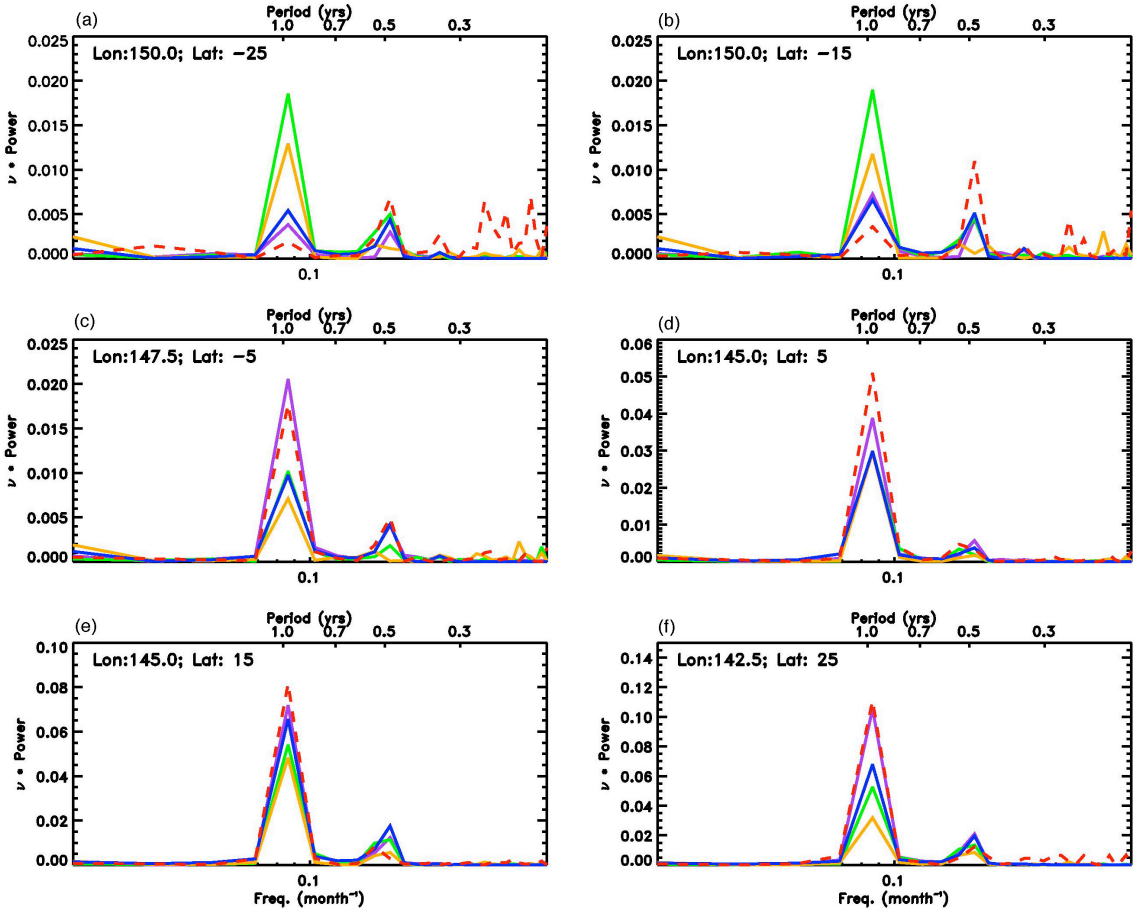

Figure 3: (a) Caltech/JPL 2-D model $CO_2$ at 25°N. (b) Seasonal cycle of model $CO_2$ at 25°N. (c) Semiannual cycle of model $CO_2$ at 25°N. Model $CO_2$ forced by the GLOBALVIEW-$CO_2$ boundary condition and NCEP2 reanalysis meteorology field are shown by solid line. Model $CO_2$ forced by the linear $CO_2$ trend boundary condition and NCEP2 reanalysis meteorology are shown by dashed line. Model $CO_2$ forced by the linear $CO_2$ trend boundary condition and climatology transport field are shown by the dotted line. Units are ppm.

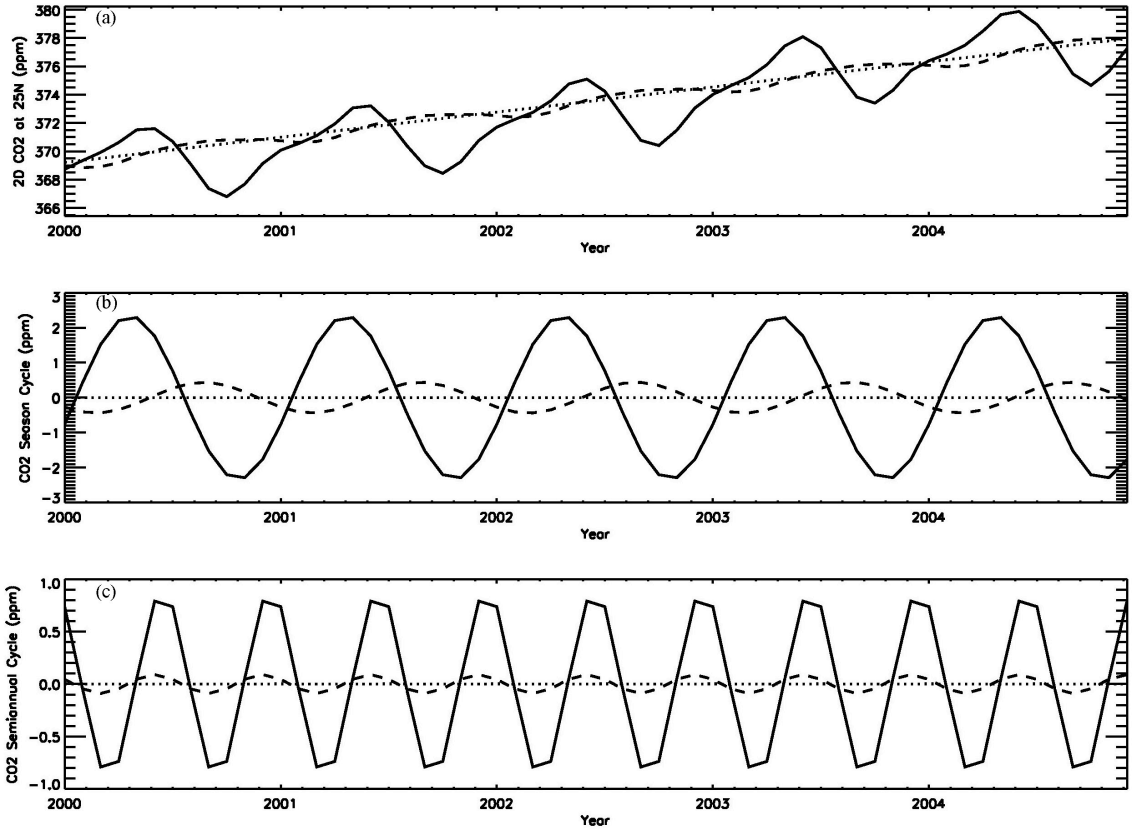

Figure 4: (a) Semi-annual oscillation amplitude from GLOBALVIEW-$CO_2$ measurement. (b) Semi-annual oscillation amplitude from GEOS-chem model $CO_2$. (c) Annual cycle amplitude from GLOBALVIEW-$CO_2$ measurement. (d) Annual cycle amplitude from GEOS-chem model $CO_2$. Units are ppm.

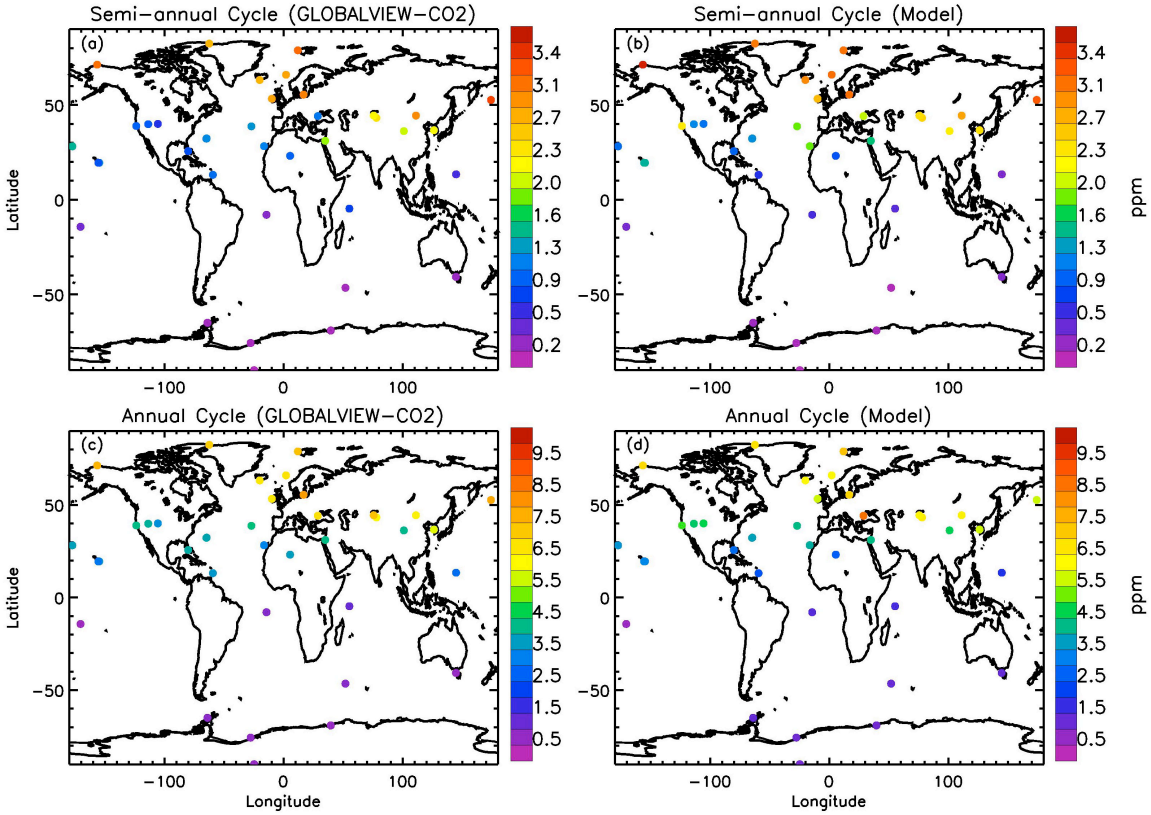

Figure 5: (a) Scatter plot of the semi-annual cycle amplitude for GLOBALVIEW-$CO_2$ and GEOS-chem model $CO_2$. (b) Scatter plot of the annual cycle amplitude for GLOBALVIEW-$CO_2$ and GEOS-chem model $CO_2$.

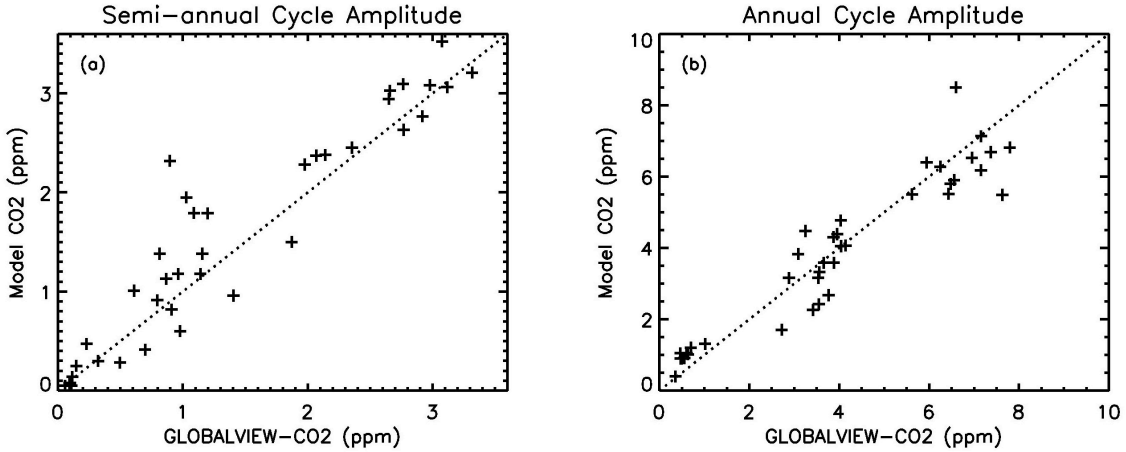

Figure 6: (a) Latitudinal distribution of semi-annual cycle amplitude. (b) Latitudinal distribution of annual cycle amplitude. Diamonds are the results from GLOBALVIEW-$CO_2$. Triangles are the results from GEOS-chem model. Error bars are the standard deviations of the results at each latitude band.

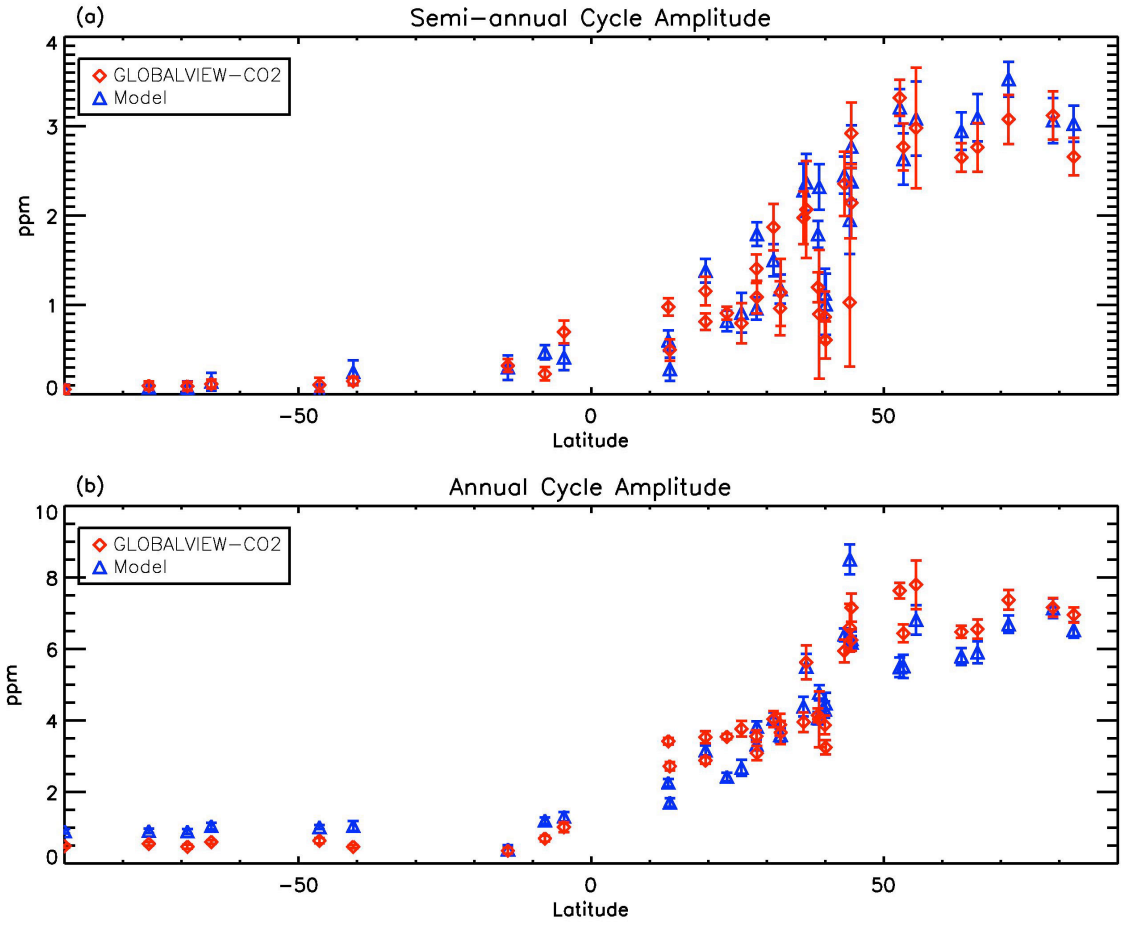

Figure 7: (a) Gross Primary Production, (b) Ecosystem Respiration, and (c) Net Ecosystem Production from Carnegie-Ames-Stanford (CASA) ecosystem model at 30°N and 110°E.